Photoelectrochemical Behavior of Self-Assembled Ag/Co Plasmonic Nanostructures Capped with TiO2

ARTICLE *in* JOURNAL OF PHYSICAL CHEMISTRY LETTERS · JANUARY 2014

Impact Factor: 7.46 · DOI: 10.1021/jz402320p

THE JOURNAL OF PHYSICAL CHEMISTRY Letters

Letter

pubs.acs.org/JPCL

Photoelectrochemical Behavior of Self-Assembled Ag/Co Plasmonic Nanostructures Capped with TiO_2

Anri Watanabe,[†] Yuki Kotake,[§] Yoshiomi Kamata,[§] Akira Chikamatsu,[†,‡] Kosei Ueno,[§] Hiroaki Misawa,[§] and Tetsuya Hasegawa*[,†,‡]

[†]Department of Chemistry, School of Science, The University of Tokyo, Tokyo 113-0033, Japan

[‡]JST-CREST, Tokyo 113-0033, Japan

[§]Research Institute for Electronic Science, Hokkaido University, Sapporo 001-0021, Japan

ABSTRACT: The use of localized surface plasmon resonance induced by Ag nanostructures is a promising way for high-efficiency photoelectric conversion. In plasmonic photoelectric conversion devices, however, the chemical instability of Ag in ambient atmosphere and its immediate deterioration have been a critical issue. Here, we propose a Ag−Co nanostructure array embedded in a TiO_2 matrix as a plasmonic resonator that ensures long-term stability. We also developed an electrochemical process to remove surface Co nanoclusters protecting fresh Ag from exposure to air. This enabled us to "unseal" Ag at the desired time. Furthermore, we confirmed photoelectric conversion using Ag−Co−TiO_2 nanocomposite films in contact with solution; the photoelectric conversion was substantially enhanced by the plasmon resonance of the Ag nanorods. The Ag nanostructures sealed in a TiO_2 matrix are expected to be used in other application fields, such as catalytisis and sensing, in which a fresh Ag surface is needed.

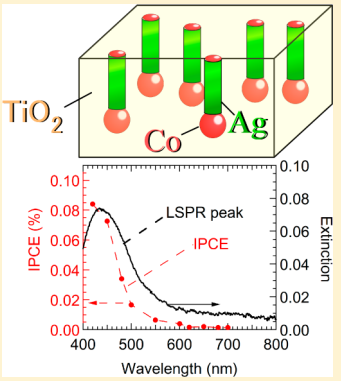

SECTION: Plasmonics, Optical Materials, and Hard Matter

Localized surface plasmon resonance (LSPR) induced by Ag nanostructures exhibits a large optical electric field enhancement due to the small imaginary part of its dielectric constant in the visible wavelength region.[1,2] The LSPR properties of Ag are expected to have promising applications, such as surface-enhanced Raman spectroscopy (SERS),[3−7] photoelectric conversion,[8−10] surface-plasmon-assisted nanolithography,[11,12] or sensing and imaging.[13]

Ag has achived photocatalytic activities using the light of longer wavelength.[14−19] Photoelectric conversion using Ag nanostructures, catalytically loaded on the surfaces of nanoporous TiO_2 films, was investigated by Tatsuma et al.[20] They found that TiO_2 films combined with Ag nanoparticles show four times higher conversion efficiency than those with Au nanoparticles. Under irradiation of light in visible wavelengths corresponding to the LSPR band of Ag nanoparticles, the Ag nanoparticles dissolved into water. This is probably because LSPR induces the photooxidation; photoexcited electrons are transferred from Ag to the conduction band of TiO_2 and, subsequently, produce Ag^+ ions dissolved in water or the electrolyte.[21]

However, the Ag−TiO_2 nanoparticle composite has a serious drawback if used as a photoelectric conversion system because the Ag nanoparticles easily sulfidate and oxidate in ambient air even if they are preserved under dark conditions, resulting in the disappearance of Ag plasmon resonance.[22] To avoid such chemical deterioration of Ag, Ag should be embedded in a matrix with low O_2 permeability, such as oxides[23] or polymers.[24] Conversely, protected Ag cannot serve as an electron donor in photoelectric conversion devices because it is not in contact with an electrolyte. Thus, it is desired to establish a procedure for preparing fresh Ag surfaces from protected Ag nanoparticles.

Recently, we succeeded in embedding Ag−Co nanostructure in anatase TiO_2 films in a self-assembled manner by depositng a mixture of Ag_2O, CoO, and TiO_2 with pulsed laser deposition (PLD). Each Ag−Co nanostructure has a characteristic nanomatch-like shape composed of a Co nanosphere and a Ag nanorod. Suprisingly, this compoiste film showed clear LSPR of the Ag nanorods in the visible wavelength region,[25] and moreover, the plasmon resonance spectrum was maintained even 6 months after film deposition. The Ag−Co nanostructure encapsuled in a TiO_2 matrix was also stable in various solvents, including water, ethanol, and acetone. Indeed, we confirmed that ultrasonic washing of the Ag−Co−TiO_2 film for more than 10 min does not affect the lifetime of the Ag−Co nanostructure at all. In addition, the Ag−Co−TiO_2 film is much easier to handle than the bare Ag nanostructures made by catalytic loading or the lithography technique.

In this study, we propose photoelecric converion using the Ag nanorods with long-term stability. The Ag nanorods are densely distributed near the TiO_2 film surface. Though most of Co is segregated between Ag nanorods and the substrate to

Received: October 28, 2013
Accepted: November 27, 2013
Published: November 27, 2013

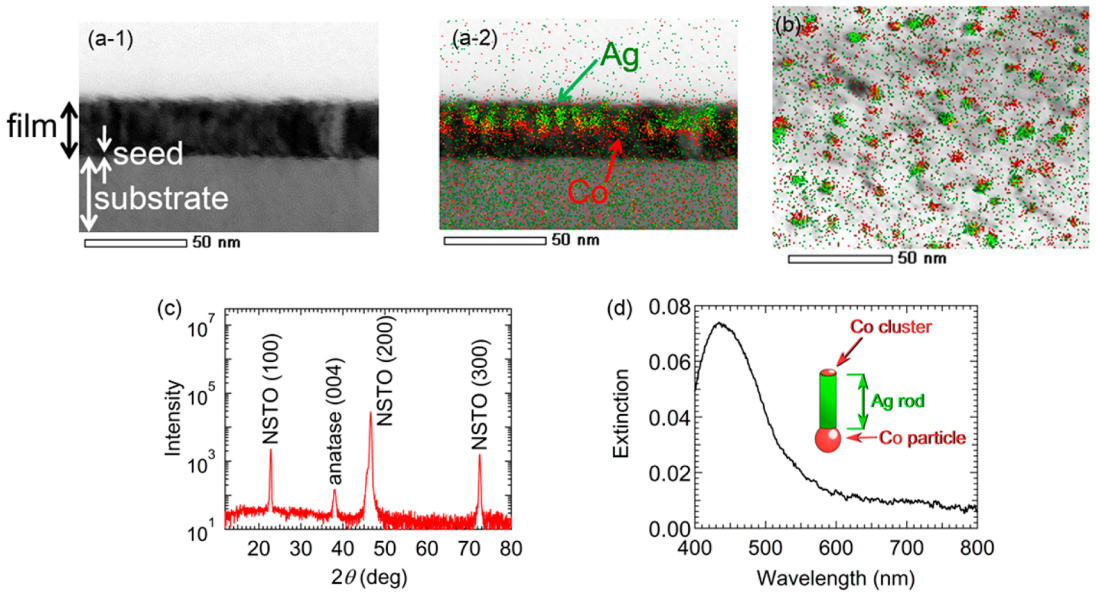

Figure 1. (a) Cross-sectional and (b) plain-view TEM-EDX images of the $Ag_6Co_3(TiO_2)_{91}$ film. (a-1) TEM image without the EDX map; (a-2) and (b) TEM images with EDX maps. Ag and Co are depicted in green and red, respectively. (c) $\theta-2\theta$ XRD pattern of the $Ag_6Co_3(TiO_2)_{91}$ film. The peaks from the Nb−STO substrate are labeled by NSTO. (d) Extinction spectrum of the $Ag_6Co_3(TiO_2)_{91}$ film. The inset schematically illustrates the shape of the Ag−Co nanostructure.

form Co nanospheres, Co nanoclusters of several nm in size also reside near the film surface and prevent direct exposure of Ag nanorods to air. The Ag−Co nanostructures sealed in a TiO_2 matrix survive at least for several months, which enables us to store them for months and to transfer them to users who need fresh Ag surfaces.

However, in order to start the photoelectric conversion, the protective Co surface layer should be removed to bring the Ag nanorods into contact with electrolyte solution. Here, we devise a removal process of the Co nanoclusters from the surface by an electrochemical process, that is, to "unseal" the protected Ag nanorods at the desired time. Furthermore, we demonstrate the potential of the Ag−Co−TiO_2 nanocomposite film as an innovative electrode in plasmonic photoelectrochemical cells or other devices such as sensors.

Figure 1a shows cross-sectional scanning transmission electron microscopy (STEM) combined with energy-dispersive X-ray spectroscopy (EDX) image of the Ag−Co−TiO_2 nanocomposite ($Ag_6Co_3(TiO_2)_{91}$) film fabricated on the Nb/TiO_2 buffer layer on a Nb−$SrTiO_3$ (Nb−STO) substrate. The typical film thickness of the top layer and the seed layer are ∼23 and ∼2 nm, respectively. The figure demonstrates the characteristic "nanomatch"-like structures composed of Co nanospheres at the bottom and Ag nanorods at the top, similar to those observed in the Ag−Co−TiO_2 film on the $LaSrAlO_4$ insulate substrate.[25] The Ag−Co nanomatch-like structures are located in the film matrix ∼5 nm apart from the seed layer. Each Ag nanorod with a dimension of ∼5 nm in diameter and ∼10 nm in length grows from a Co nanosphere toward the film surface. The formation mechanism of the Ag−Co nanostructures was reported previously.[25] Tiny Co nanoclusters on the film surface prevent the Ag nanorods from exposure to air. That is, each Ag nanorod is sandwiched by a Co nanosphere at the bottom and a Co nanocluster on the top. As seen from the plain-view STEM-EDX image shown in Figure 1b, the lateral positions of the nanororods in the film are random, and the averaged interval between adjacent nanomatches is 10−20 nm.

Figure 1c shows a $\theta-2\theta$ X-ray diffraction (XRD) pattern of the $Ag_6Co_3(TiO_2)_{91}$ film. The XRD pattern clearly indicates a diffraction peak at $2\theta \approx 38°$, corresponding to the (004) reflection of anatase TiO_2. No secondary phases, such as Co and Ag, were detected, reflecting that Co and Ag are present in the form of nanoparticles. The anatase (004) diffraction appeared as a spot in the $2\theta-\chi$ image measured with a two-dimensional detector (data not shown), proving that the matrix is in the single-crystalline anatase phase with a high degree of crystallinity. Figure 1d depicts the extinction spectrum of the $Ag_6Co_3(TiO_2)_{91}$ film. A broad LSPR band due to randomly dispersed Ag nanostructures is seen at around 400−600 nm. The higher dielectric constant of the surrounding TiO_2 matrix results in the enhanced LSPR peak and the red shift of its peak position.[26−28]

Meanwhile, for photoelectric conversion, the Ag nanorods need to be in contact with an electrolyte solution. In fact, no photocurrent was observed for the pristine Ag−Co−TiO_2 nanocomposite film whose surface was covered by Co nanoclusters. In order to bring the Ag nanorods into contact with the electrolyte, we tried to remove the Co nanoclusters on the film surface by selective electrochemical oxidation of Co. To dissolve preferentially surface Co nanoclusters, a voltage of 0.3 V versus a saturated calomel electrode (SCE) was applied to the working electrode for 100 s under darkness. Hereafter, we refer to this process as initialization. Figure 2a shows the linear sweep voltammogram measured after initialization with and without irradiation of the light ($420 < \lambda \leq 1300$ nm). As seen from the figure, the current is enhanced under the irradiation, representing the anodic photocurrent. Figure 2b shows amperometric $I-t$ curves before and after initialization under irradiation of light at $\lambda = 450$ nm, where the working electrode potential (V) was set to 0.1 V versus SCE. Both curves show a clear photocurrent in response to the illumination of light. The $I-t$ curve before initialization was almost the same as that of the pure TiO_2 film. In contrast, the photocurrent after initialization was enhanced seven times. This proves that the

dx.doi.org/10.1021/jz402320p | J. Phys. Chem. Lett. 2014, 5, 25−29

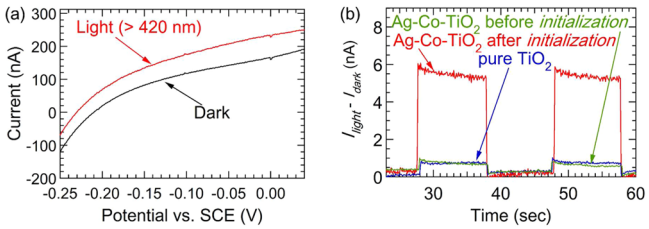

Figure 2. (a) Linear sweep voltammogram with and without light irradiation after initialization. The sweep rate was 0.05 V/s. (b) Amperometric $I-t$ curves before and after initialization under irradiation of light (λ = 450 nm). The working electrode potential (V) was set to 0.1 V versus SCE.

Ag nanorods originally "sealed" in a TiO_2 matrix by surface Co nanoclusters were successfully unsealed by the initialization process. Co and Ag contents that were dissolved into solution during the initialization process were evaluated to be ~5.5 and ~10% of the total Co and Ag content, respectively, by inductively coupled plasma mass spectrometry (ICP-MS). This indicates that nanoscale channels were formed between Ag nanorods and the electrolyte solution due to the dissolution of surface Co metal nanoclusters. Accordingly, during the initialization process (generated by a 0.3 V versus SCE relative to the working electrode in the neutral solution), not only Co but also Ag was oxidized and dissolved into the soluion.[29] As described above, Ag showed a higher dissolution rate than Co during the initialization. This is probably because Ag is densely distributed near the film surface, while most of the Co exists at the substrate side. Only a small amount of Co located near the surface could dissolve into the solution during the initialization. It is suggested that once Ag is in contact with the electrolyte solution, a photocurrent is observed due to photooxidation based on plasmon-induced charge separation, and simultaneously, the Ag^+ ions produced by photooxidation dissolve into the solution.

Figure 3 compares the incident photon-to-photocurrent efficiency (IPCE) action spectrum and the plasmon resonance

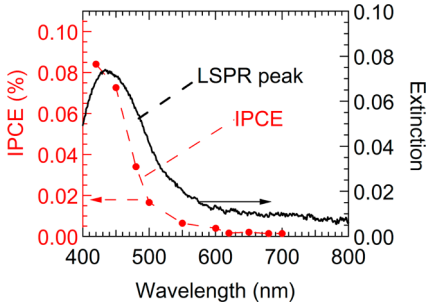

Figure 3. IPCE action spectrum (red dotted line) and plasmon resonance spectrum (black solid line) of the $Ag_6Co_3(TiO_2)_{91}$ film.

spectrum of the $Ag_6Co_3(TiO_2)_{91}$ film. Notably, both spectra show similar behavior, that is, an abrupt increase of extinction/IPCE with decreasing wavelength below 600 nm. This strongly suggests that the photocurrent was enhanced by the effect of plasmon resonace. However, both spectra show inconsistency at the shorter wavelength region; the extinction spectrum has a peak at around λ = 440 nm, while IPCE is monotonically increased with decreasing wavelength. One possible explanation for the λ = 420 nm is that an interband transition of TiO_2 itself contributed to IPCE. The band gap of pure TiO_2 is 3.2 eV, which corresponds to ~390 nm. The present TiO_2-based film contains a certain amount of oxygen vacancies because of the deposition under a reducing atmosphere. The oxygen vacancies form n-type impurity states near the bottom of the TiO_2 conduction band, which effectively reduces the band gap of TiO_2. However, the IPCE value of the pure TiO_2 film without Ag and Co was smaller than 0.01%. Thus, the interband transition cannot solely account for the large enhancement of photocurrent at 420 nm. Considering the fact that the tail of the TiO_2 band edge overlaps with the LSPR peak, we speculate that the interaction between interband excitation and LSPR substantially enhances the photocurrent.

After continuous electrochemical measurements under irradiation (λ = 450 nm) for 14 h, the LSPR peak of Ag in the extinction spectrum completely disappeared, and no Ag or Co peaks were detected in STEM-EDX measurements. The disappearance of Ag and Co was due to photoelectrochemical reaction, and the chemical deterioration, that is, sulfidation and oxidation, in ambient conditions during several tens of hours can be neglected. The total Ag amount, estimated from the photocurrent value, was 90% of that contained in the whole film. This value is reasonable because about 10% of Ag was dissolved into the solution during the initialization process. As a consequence of the present study, we speculate the following photoelectric conversion mechanism. First, LSPR of Ag is induced, and then, the excited electrons of Ag are transferred to the conduction band of TiO_2. Accompaning the appearance of a photocurrent, photooxidized Ag dissolves into electrolyte in the form of Ag^+ ions.

Finally, we argue on the possible applications of the present Ag−Co nanostructure embedded in a TiO_2 matrix. A promising way to use it is efficient photoelectric conversion assisted by LSPR, as described above. The Ag−Co nanostructure can be stored until its use, and it can be unsealed just before starting photoelectric conversion, which is advantageous over the conventional cells using bare Ag. However, there is a limitation to the operation time because Ag dissolves into aqueous solution. Thus, disposable and portable plasmonic cells are promising targets of the Ag−Co−TiO_2 film. A problem is that Ag is easier to be oxidized than water. However, if a reductive reagent, which is easier to be oxidized than Ag, is added to the solution, Ag no longer dissolves, and the cells can be used in a half-eternal manner.

Other potential applications are biosensors by using SERS. Again, the fresh Ag surface can be prepared just prior to the sensing because bare silver is soon deteriorated in solutions, and coated Ag is often used for SERS in the solutions. However, from a viewpoint of sensitivity as a sensor, it is better for biomolecules to interact with fresh Ag directly. Thus, the protection of Ag and the sensitivity are in a relationship of trade-off. Once the Ag structure is coated by conventional materials, such as SiO_2 and polymer, it is difficult to remove the coating. In the Ag−Co nanostructures encapsulated in TiO_2, a fresh Ag surface can be prepared by removing the "coating" just before the measurement. Therefore, the present Ag−Co−TiO_2 system enables both Ag protection and high sensitivity, which is of great advantage over conventional sensors using bare and coated Ag.

In summary, we propose an electrochemical process to unseal Ag nanorod structures embedded in a TiO_2 matrix. A direct contact of the Ag nanorods with the supporting electrolyte after the unseal process was confirmed by the observation of a photocurrent. On the basis of the IPCE and

dx.doi.org/10.1021/jz402320p | J. Phys. Chem. Lett. 2014, 5, 25−29

extinction spectral measurements, it was revealed that photoelectric conversion was substantially enhanced by plasmon resonance of Ag nanorods. These results raise the hope that the Ag nanostructures sealed in a TiO_2 matrix can be used not only in plasmonic devices but also in other application fields, such as catalytisis and sensing, in which a fresh Ag surface is needed.

EXPERIMENTAL METHODS

Ag−Co−TiO_2 nanocompsoite films were fabricated on a Nb 0.5 wt % or a Nb 0.05 wt % doped STO(100) substrate by the PLD method. A KrF excimer laser (λ = 248 nm) with a frequency of 2 Hz and an energy of 18 mJ/pulse was used for ablation. Sintered pellets of $Ti_{0.97}Nb_{0.03}O_2$ and a mixture of $Ag_2O/CoO/TiO_2$ = 10:5:95, $Ag_{20}Co_5(TiO_2)_{95}$, were used as PLD targets for seed layers and Ag−Co−TiO_2 nanocomposite films, respectively. A Nb 3% doped anatase TiO_2 seed layer was first deposited on the Nb−STO(100) substrate at a substrate temperature (T_s) of 650 °C and an oxygen partial pressure (P_{O_2}) of 1 × 10^{-5} Torr.[30] Then, a Ag−Co−TiO_2 nanocompsoite thin film was deposited on the seed layers at T_s = 300 °C and P_{O_2} = 1 × 10^{-6} Torr. The composition of the Ag−Co−TiO_2 nanocomposite film was evaluated to be $Ag_6Co_3(TiO_2)_{91}$ by ICP-MS (Thermo Scientific, XSeries2 ICP-MS equipped with a New Wave, UP-213 laser ablation system). Cross-sectional and plain-view images were taken by bright-field STEM (JEOL, JEM-2100F HC) combined with EDX. Crystal structures of the films were characterized by a XRD spectrometer with a two-dimensional detector (Bruker, AXS with GADDS). The extinction spectrum measurements were performed using a microscopic absorption spectroscopic measurement system. A collimated beam from a halogen lamp mounted on an optical microscope (BX-51, Olympus Co.) was employed as a probe light source for the extinction spectrum measurements. The beam was collimated using a condenser lens of the microscope. The transmitted beam was collected using a 10× microscope objective lens (with a numerical aperture of 0.3). The probe beam was subsequently coupled to a multichannel photodetector (PMA-11, Hamamatsu Photonics K.K.) after passing through a pinhole (φ: 1.0 mm). The recorded spectra were normalized to the spectrum of the incident beam.

Photoelectrochemical measurements were performed using a three-electrode electrochemical measurement system. The $Ag_6Co_3(TiO_2)_{91}$ film, a platinum wire, and a SCE were used as working, counter, and reference electrodes, respectively.[31] As an electrolyte solution, an Ar-saturated 0.1 M $KClO_4$ aqueous solution was used without any electron donors. The working electrode was set in a Teflon cell for electrochemical measurements. The light was introduced through an optical window (φ: 2 mm) of this cell. As the light source, a xenon lamp (Xenon Research Arc Lamp Sources, Newport Co.) was used, and the irradiation wavelength was selected by a band-pass filter or a long-pass filter. For the IPCE measurements, the light was monochromatized by band-pass filters (full width at half-maximum = 10 nm). To extract the photocurrent from the working electrode, the Nb−STO substrate was back-contacted with an In−Ga alloy paste to achieve an ohmic contact.

AUTHOR INFORMATION

Corresponding Author

*E-mail: hasegawa@chem.s.u-tokyo.ac.jp.

Notes

The authors declare no competing financial interest.

ACKNOWLEDGMENTS

A part of this work was conducted at the Research Hub for Advanced Nano Characterization and at the Center for Nano Lithography & Analysis, University of Tokyo, supported by the Ministry of Education, Culture, Sports, Science and Technology (MEXT), Japan.

REFERENCES

(1) Kreibig, U.; Vollmer, M. *Optical Properties of Metal Clusters*; Springer-Verlag: New York, 1995.
(2) Kelly, K. L.; Coronado, E.; Zhao, L. L.; Schatz, G. C. The Optical Properties of Metal Nanoparticles: The Influence of Size, Shape, and Dielectric Environment. *J. Phys. Chem. B* **2003**, *107*, 668−677.
(3) Haynes, C. L.; Van Duyne, R. P. Plasmon-Sampled Surface-Enhanced Raman Excitation Spectroscopy. *J. Phys. Chem. B* **2003**, *107*, 7426−7433.
(4) Fang, Y.; Seong, N. H.; Dlott, D. D. Measurement of the Distribution of Site Enhancements in Surface-Enhanced Raman Scattering. *Science* **2008**, *321*, 388−392.
(5) Fleischmann, M.; Hendra, P. J.; McQuilla, A. J. RAMAN-Spectra of Pyridine Adsorbed at a Silver Electrode. *Chem. Phys. Lett.* **1974**, *26*, 163−166.
(6) Jeanmaire, D. L.; Vanduyne, R. P. Surface Raman Spectroelectrochemistry: Part I. Heterocyclic, Aromatic, and Alphatic Amines Adsorbed on Anodized Silver Electrode. *J. Electroanal. Chem.* **1977**, *84*, 1−20.
(7) Albrecht, M. G.; Creighton, J. A. Anomalously Intense Raman Spectra of Pyridine at A Silver Electrode. *J. Am. Chem. Soc.* **1977**, *99*, 5215−5217.
(8) Westphalen, M.; Kreibig, U.; Rostalski, J.; Luth, H.; Meissner, D. Metal Cluster Enhanced Organic Solar Cells. *Sol. Energy Mater.* **2000**, *61*, 97−105.
(9) Kulkarni, A. P.; Noone, K. M.; Munechika, K.; Guyer, S. R.; Ginger, D. S. Plasmon-Enhanced Charge Carrier Generation in Organic Photovoltaic Films Using Silver Nanoprisms. *Nano Lett.* **2010**, *10*, 1501−1505.
(10) Yoon, W. J.; Jung, K. Y.; Liu, J. W.; Duraisamy, T.; Revur, R.; Teixeira, F. L.; Sengupta, S.; Berger, P. R. Plasmon-Enhanced Optical Absorption and Photocurrent in Organic Bulk Heterojunction Photovoltaic Devices Using Self-Assembled Layer of Silver Nanoparticles. *Sol. Energy Mater.* **2010**, *94*, 128−132.
(11) Srituravanich, W.; Durant, S.; Lee, H.; Sun, C.; Zhang, X. Deep Subwavelength Nanolithography Using Localized Surface Plasmon Modes on Planar Silver Mask. *J. Vac. Sci. Technol., B* **2005**, *23*, 2636−2639.
(12) Luo, X. G.; Ishihara, T. T. Surface Plasmon Resonant Interference Nanolithography Technique. *Appl. Phys. Lett.* **2004**, *84*, 4780−4782.
(13) Lee, K. S.; El-Sayed, M. A. Gold and Silver Nanoparticles in Sensing and Imaging: Sensitivity of Plasmon Response to Size, Shape, and Metal Composition. *J. Phys. Chem. B* **2006**, *110*, 19220−19225.
(14) Yu, J. G.; Dai, G. P.; Huang, B. B. Fabrication and Characterization of Visible-Light-Driven Plasmonic Photocatalyst $Ag/AgCl/TiO_2$ Nanotube Arrays. *J. Phys. Chem. C* **2009**, *113*, 16394−16401.
(15) Awazu, K.; Fujimaki, M.; Rockstuhl, C.; Tominaga, J.; Murakami, H.; Ohki, Y.; Yoshida, N.; Watanabe, T. A Plasmonic Photocatalyst Consisting of Sliver Nanoparticles Embedded in Titanium Dioxide. *J. Am. Chem. Soc.* **2008**, *130*, 1676−1680.
(16) Christopher, P.; Ingram, D. B.; Linic, S. Enhancing Photochemical Activity of Semiconductor Nanoparticles with Optically Active Ag Nanostructures: Photochemistry Mediated by Ag Surface Plasmons. *J. Phys. Chem. C* **2010**, *19*, 9173−9177.

(17) Zhou, X.; Hu, C.; Hu, X.; Peng, T.; Qu, J. Plasmon-Assisted Degradation of Toxic Pollutants with Ag−AgBr/Al_2O_3 under Visible-Light Irradiation. *J. Phys. Chem. C* **2010**, *114*, 2746−2750.
(18) Kumar, M. K.; Krishnamoorthy, S.; Tan, L. K.; Chiam, S. Y.; Tripathy, S.; Gao, H. Field Effects in Plasmonic Photocatalyst by Precise SiO_2 Thickness Control Using Atomic Layer Deposition. *ACS Catal.* **2011**, *1*, 300−308.
(19) Ingram, D. B.; Linic, S. Water Splitting on Composite Plasmonic−Metal/Semiconductor Photoelectrodes: Evidence for Selective Plasmon-Induced Formation of Charge Carriers near the Semiconductor Surface. *J. Am. Chem. Soc.* **2011**, *133*, 5202−5205.
(20) Tian, Y.; Tatsuma, T. Plasmon-Induced Photoelectrochemistry at Metal Nanoparticles Supported on Nanoporous TiO_2. *Chem. Commun.* **2004**, *16*, 1810−1811.
(21) Naoi, K.; Ohko, Y.; Tatsuma, T. TiO_2 Films Loaded with Silver Nanoparticles: Control of Multicolor Photochromic Behavior. *J. Am. Chem. Soc.* **2004**, *126*, 3664−3668.
(22) Wang, L.; Xiong, W.; Nishijima, Y.; Yokota, Y.; Ueno, K.; Misawa, H.; Bi, G.; Qiu, J. R. Spectral Properties and Mechanism of Instability of Nanoengineered Silver Blocks. *Opt. Express* **2011**, *19*, 10640−10646.
(23) Szunerits, S.; Castel, X.; Boukherroub, R. Surface Plasmon Resonance Investigation of Silver and Gold Films Coated with Thin Indium Tin Oxide Layers: Influence on Stability and Sensitivity. *J. Phys. Chem. C* **2008**, *112*, 15813−15817.
(24) Manickam, G.; Gandhiraman, R.; Vijayaraghavan, R. K.; Kerr, L.; Doyle, C.; Williams, D. E.; Daniels, S. Protection and Functionalisation of Silver as an Optical Sensing Platform for Highly Sensitive SPR Based Analysis. *Analyst.* **2012**, *137*, 5265−5271.
(25) Watanabe, A.; Ikemiya, K.; Chikamatsu, A.; Hirose, Y.; Hasegawa, T. Structural Variation in Ag−Co Nanostructures Embedded in TiO_2 Thin Films Fabricated by Pulsed Laser Deposition. *Chem. Lett.* **2013**, DOI: 10.1246/cl.130903.
(26) Shi, W. L.; Zeng, H.; Sahoo, Y.; Ohulchanskyy, T. Y.; Ding, Y.; Wang, Z. L.; Swihart, M.; Prasad, P. N. A General Approach to Binary and Ternary Hybrid Nanocrystals. *Nano Lett.* **2006**, *6*, 875−881.
(27) Novo, C.; Funston, A. M.; Pastoriza-Santos, I.; Liz-Marzan, L. M.; Mulvaney, P. Influence of the Medium Refractive Index on the Optical Properties of Single Gold Triangular Prisms on a Substrate. *J. Phys. Chem. C* **2008**, *112*, 3−7.
(28) Malinsky, M. D.; Kelly, K. L.; Schatz, G. C.; Van Duyne, R. P. Chain Length Dependence and Sensing Capabilities of the Localized Surface Plasmon Resonance of Silver Nanoparticles Chemically Modified with Alkanethiol Self-Assembled Monolayers. *J. Am. Chem. Soc.* **2001**, *123*, 1471−1482.
(29) Pourbaix, M. *Atlas of Electrochemical Equilibria in Aqueous Solutions*; National Association of Corrosion Engineers: Houston, TX, 1974; Sections 12.2 and 14.2.
(30) Nogawa, H.; Chikamatsu, A.; Hirose, Y.; Nakao, S.; Kumigashira, H.; Oshima, M.; Hasegawa, T. Carrier Compensation Mechanism in Heavily Nb-Doped Anatase $Ti_{1-x}Nb_xO_{2+\delta}$ Epitaxial Thin Films. *J. Phys. D: Appl. Phys.* **2011**, *44*, 365404.
(31) Nishijima, Y.; Ueno, K.; Yokota, Y.; Murakoshi, K.; Misawa, H. Plasmon-Assisted Photocurrent Generation from Visible to Near-Infrared Wavelength Using a Au-Nanorods/TiO_2 Electrode. *J. Phys. Chem. Lett.* **2010**, *1*, 2031−2036.